ELSEVIER

Physica B 221 (1996) 18–26

PHYSICA B

Probing interface roughness by X-ray scattering

Dick K.G. de Boer*, Ann J.G. Leenaers

Philips Research Laboratories, Prof. Holstlaan 4, 5656 AA Eindhoven, The Netherlands

Abstract

X-ray scattering at glancing angles can be exploited to probe interface roughness. Various theories for this technique will be reviewed. The applicability of the theories is shown to depend on the relevant length scales of sample and X-rays. Approximations are discussed and improvements of the theory are suggested. Both specular reflection, diffuse scattering and absorption of X-rays will be discussed. It will be shown that relevant roughness parameters, like root-mean-square roughness, lateral and perpendicular correlation lengths and the degree of jaggedness can be extracted from the experiments. Possible forms for the roughness correlation function are discussed. As an example, it is shown how the interface roughness of an oxidic multilayer has been probed by X-ray scattering.

1. Introduction

In the last decade there has been a growing interest to manipulate the properties of materials by depositing them as thin layers or multilayers on a substrate. The properties of the resulting devices are determined to a large extent by the roughness of the interfaces.

As can be concluded from the previous conferences in this series [1, 2], X-ray scattering at glancing angles is a powerful tool to probe interface roughness. Specular reflectivity is sensitive to the depth profile of a sample and can yield the root-mean-square (rms) roughness. The diffuse scattering measured in non-specular directions can give information on the nature of the roughness along the interfaces.

In this paper we will give a review of the physical background of these measurements. We will compare various theories and indicate their applicability and limitations. An example will be given of the determination of roughness parameters for a multilayered sample and we will refer to other examples from the literature.

2. Scattering theory

We will give an overview of the theory for glancing-incidence X-ray scattering from a sample with rough interfaces. Most of the theory will apply to neutron scattering as well, although for neutrons one generally can neglect absorption. An extensive treatment of the theory in the case of small roughness correlation lengths was published recently [3]. Here we will concentrate more on the applicability of the theory.

First we will discuss the case of very small correlation lengths, where diffuse scattering can be neglected. Then we will show how perturbation theory can be used in the case of larger correlation lengths. We will find that this approach breaks down if the correlation lengths are too large. Other limitations may be encountered if the rms roughness is too large, in which case another starting point for the perturbation theory can be used favourably. Finally, we will discuss an approach which is valid for large correlation lengths.

At small scattering angles, where it is allowed to neglect the polarisation of the X-rays, the electric fields ϕ are solutions of the wave equation

$$(\nabla^2 + k^2 - V)\phi = 0, \tag{1}$$

where $k = 2\pi/\lambda$ is the magnitude of the wave vector of the incident X-rays with wavelength λ and the effective potential is $V = k^2(1 - n^2)$, where the refractive index n depends on the position in the sample. We will not be concerned with the atomic structure of the material, which is justified as long as $\lambda/\sin\theta$ is much larger than the atomic distances, where θ is the angle of incidence with the sample surface.

* Corresponding author.

0921-4526/96/$15.00 © 1996 Elsevier Science B.V. All rights reserved
SSDI 0921-4526(95)00900-0

We will assume that a rough interface can be characterised by an rms roughness σ and a lateral roughness correlation length ξ. The lateral distance over which the interface height fluctuations have to be averaged to obtain σ is approximately equal to the X-ray coherence length. If the interface roughness profile is viewed as a Fourier series, the roughness correlation length ξ can be seen as a largest typical period in it.

It is instructive to consider first X-ray scattering at an interface with the shape of a simple grating with grating period D. If an X-ray beam with wavelength λ impinges on such a grating at incidence angle θ, there will be diffracted beams at angles θ_d fulfilling the grating equation $n\lambda = D(\cos\theta_d - \cos\theta)$. Since the smallest period which can give diffraction is that for which $\theta_d = 0$, no diffraction is possible if $D < \lambda/(1 - \cos\theta)$. On the other hand, if $D \gg \lambda/(1-\cos\theta)$, many diffraction peaks will occur very close to the specular condition $\theta_d = \theta$.

A rough interface profile contains many periods and the diffraction peaks will merge into a diffuse scattering peak. Analogously to the above situation, the diffuse scattering will be small if $\xi < \lambda/(1-\cos\theta)$ and can be neglected if $\xi \ll \lambda/(1-\cos\theta)$. In the opposite case, $\xi \gg \lambda/(1-\cos\theta)$, the diffuse scattering will be large but will occur very close to the specular condition.

In the case $\xi \ll \lambda/(1-\cos\theta)$ it is allowed to use a laterally averaged refractive-index depth profile. That is, the situation is that of a graded interface. If the interface has a normal distribution of height deviations, the depth profile is an error function. For that case the wave equation cannot be solved exactly, but a numerical solution can be obtained using the slice method [4]. Below also an approximate solution for this case will be discussed, Eq. (5).

In the following we will assume that the potential of Eq. (1) can be written as

$$V = V_0 + V_1, \tag{2}$$

where V_0 has no lateral dependence and V_1 describes the local interface position. Here we will consider two situations for V_0: that corresponding to flat interfaces and that corresponding to graded interfaces.

Formally, the solution of Eq. (1) now can be written as

$$\phi = \phi_0 + G_0 V_1 \phi, \tag{3}$$

where ϕ_0 is the solution of Eq. (1) for the potential V_0 and G_0 is the corresponding Green's function. The formal notation of the last term in Eq. (3) implies an integral over all space. However, only the interfacial regions contribute to the integral, since V_1 is zero elsewhere.

First we will consider the case in which V_0 corresponds to the situation of flat interfaces (which are assumed to be parallel in a multilayer). Then, for an interface located at $z = 0$, the solution for ϕ_0 is

$$\phi_0 = \begin{cases} [\exp(\mathrm{i}k_0 z) + r_k^0 \exp(-\mathrm{i}k_0 z)]\exp(\mathrm{i}\boldsymbol{k}_\parallel \cdot \boldsymbol{x}) \\ \quad \text{for } z \geqslant 0, \\ t_k^0 \exp(\mathrm{i}k_1 z)\exp(\mathrm{i}\boldsymbol{k}_\parallel \cdot \boldsymbol{x}) \\ \quad \text{for } z \leqslant 0, \end{cases} \tag{4}$$

where $\boldsymbol{k}_\parallel$ is the component of the wave vector parallel to the interfaces, k_0 and k_1 are its perpendicular components above and below the interface, respectively, and r_k^0 and t_k^0 are the Fresnel coefficients for reflection and transmission, respectively.

First we will consider the case $\xi \ll \lambda/(1-\cos\theta)$ [5–7], that is, diffuse scattering is neglected. To solve Eq. (3), it is assumed that the solution ϕ can be written analogously to Eq. (4), but with a reflection coefficient r_k and a transmission coefficient t_k which have to be found in a self-consistent way. To perform the integral which is implicit in Eq. (3), the fields in the interfacial regions are approximated by just one of the two expressions of Eq. (4). This is justified up to $O(k_0^2\sigma^2)$ and up to $O(k_c^2/k_0^2)$, where k_c is the critical wave vector (equal to the real part of $V_0^{1/2}$). Then one obtains, after configurational averaging over a normal distribution of height deviations:

$$r_k = r_k^0 \exp(-2k_0 k_1 \sigma^2),$$
$$t_k = t_k^0 \exp[(k_0 - k_1)^2\sigma^2/2] \quad \text{if } \xi \ll \lambda/(1-\cos\theta). \tag{5}$$

For r_k the answer does not depend on which of the two expressions in Eq. (4) is taken. For t_k a somewhat different expression can be found [7], which is the same as Eq. (5) up to the order indicated above and, moreover, gives nearly the same numerical values for other k_0 values. Expressions like Eq. (5) are also valid for each interface in a multilayer [9], provided that for all interfaces $\xi \ll \lambda/(1-\cos\theta)$.

As was mentioned above, the same expressions, Eq. (5), are valid for a graded error-function profile. There is a good agreement with the values calculated using the slice method. For the reflectivity $|r_k|^2$ this can be seen in Fig. 1, where the solid line has been calculated using the slice method and the dotted line using the self-consistent solution, Eq. (5). The case of transmission will be discussed below (Fig. 4). To see the effect of the approximations made, we show in Fig. 2 the electric-field intensity as a function of depth for a case where $k_0\sigma$ is not small and k_0 is close to the critical wave vector. It is seen that, not too close to the interface, there is a good agreement between the fields calculated using the slice method (solid line) and the self-consistent solution (dotted). At the position of the flat interface, however, the self-consistent solution exhibits a discontinuity, whereas that calculated with the slice method is continuous, as it should. This means that one has to be very careful in applying the self-consistent solution close to an interface.

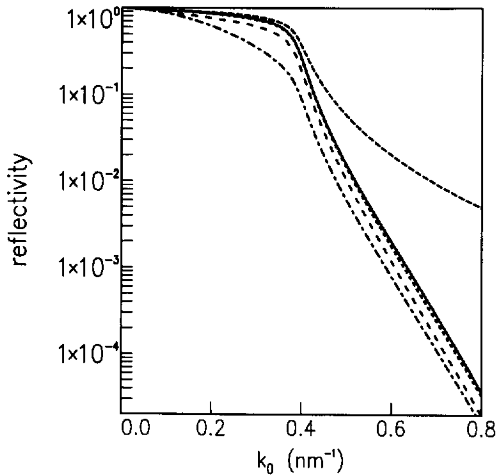

Fig. 1. Specular reflectivity versus perpendicular incident wave vector for CuKα radiation scattered from a rough platinum sample with rms roughness $\sigma = 1.5$ nm. (Dashed line) no roughness; (solid line) calculated for error-function profile; (dotted line) calculated using Eq. (5); (widely dashed line) calculated using Eq. (11) with $\xi = 100$ nm; (dot-dashed line) calculated using Eq. (12).

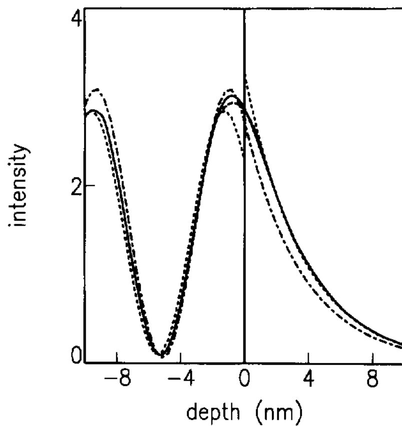

Fig. 2. Relative intensity versus depth near the surface of a platinum sample with $\sigma = 1.5$ nm due to CuKα radiation with $k_0 = 0.38\ \mathrm{nm}^{-1}$. (Dot-dashed line) no roughness; (dotted line) calculated using Eq. (5); (solid line) calculated for error-function profile; (dashed line) continuous interpolation of dotted line in interfacial region.

Next we consider the case in which ξ is larger and diffuse scattering cannot be neglected. Then one can use perturbation theory to obtain an approximate solution of Eq. (1). Considering V_1 as a perturbation on V_0, one can write

$$\phi = \phi_0 + G_0 V_1 \phi_0 + G_0 V_1 G_0 V_1 \phi_0 + \cdots . \tag{6}$$

This approach is called the distorted-wave Born approximation (DWBA), whereas in the case $V_0 = 0$ it is called the Born approximation.

The diffuse-scattering intensity can be calculated using the first-order term ($G_0 V_1 \phi_0$) of Eq. (6). Again, in the interfacial region, the fields are approximated by one of the two expressions (that for $z \leqslant 0$) of Eq. (4). For a single rough interface, the result for the differential cross section [8] is

$$\frac{\mathrm{d}\sigma}{\mathrm{d}\Omega} = APS(\boldsymbol{p}_{\parallel} - \boldsymbol{k}_{\parallel}, p_{\mathrm{l}} + k_{\mathrm{l}}), \tag{7}$$

where $\boldsymbol{k}$ is the incident wave vector, $\boldsymbol{p}$ is the scattered wave vector, A is the irradiated detected sample area and the prefactor is

$$P = k^2 |1 - n^2|^2 |t_k^0|^2 |t_p^0|^2 / (16\pi^2). \tag{8}$$

In the case of a normal distribution of height deviations $h(\boldsymbol{x})$, the structure factor is

$$S(\boldsymbol{q}_{\parallel}, q_{\perp}) = |\exp(-q_{\perp}^2 \sigma^2/2)/q_{\perp}|^2 \times \int \mathrm{d}^2\boldsymbol{X} \exp(\mathrm{i}\boldsymbol{q}_{\parallel} \cdot \boldsymbol{X}) \{\exp[|q_{\perp}|^2 C(\boldsymbol{X})] - 1\}, \tag{9}$$

where $C(\boldsymbol{X}) = \langle h(\boldsymbol{x}) h(\boldsymbol{x} + \boldsymbol{X})\rangle$ is the height–height correlation function of the rough interface (the averaging is over $\boldsymbol{x}$). Below we will discuss possible forms of $C(\boldsymbol{X})$, but in general it has the value σ^2 at $\boldsymbol{X} = 0$ and decays to zero for large $|\boldsymbol{X}|$, with ξ as characteristic decay length. In the case that $q_{\perp}\sigma$ is small, $S(\boldsymbol{q}_{\parallel}, q_{\perp})$ is approximately equal to

$$\tilde{C}(\boldsymbol{q}_{\parallel}) \equiv \int \mathrm{d}^2\boldsymbol{X} \exp(\mathrm{i}\boldsymbol{q}_{\parallel} \cdot \boldsymbol{X}) C(\boldsymbol{X}), \tag{10}$$

i.e., the power spectral density of the rough interface.

Other structure factors are more appropriate for non-normal distributions of height deviations, such as interfaces decorated with islands [10]. In the case of stepped interfaces also another structure factor can be derived, but often Eq. (9) effectively describes the roughness [11].

For multilayers the diffuse scattering can be calculated in a similar way [12], leading to a rather complicated result [13]. The formula for the cross section contains a double sum over all interfaces of eight structure factors similar to Eq. (9) with correlation functions between the height deviations of interfaces i and j, $C_{ij}(\boldsymbol{X}) = \langle h_i(\boldsymbol{x}) h_j(\boldsymbol{x} + \boldsymbol{X})\rangle$. Each structure factor has a prefactor like Eq. (8) which involves the transmitted and reflected fields at the various interfaces. The presence of these factors gives rise to interference effects which modulate the diffuse scattered intensity (see Section 5).

In the case of the Born approximation ($V_0 = 0$), similar expressions are obtained. Since refraction is neglected, the transmission coefficients in the prefactor of Eq. (7) are equal to 1, whereas the structure factor is $S(\boldsymbol{p}_{\parallel} - \boldsymbol{k}_{\parallel}, p_0 + k_0)$ [8]. For a multilayer the expression is much simpler than in the

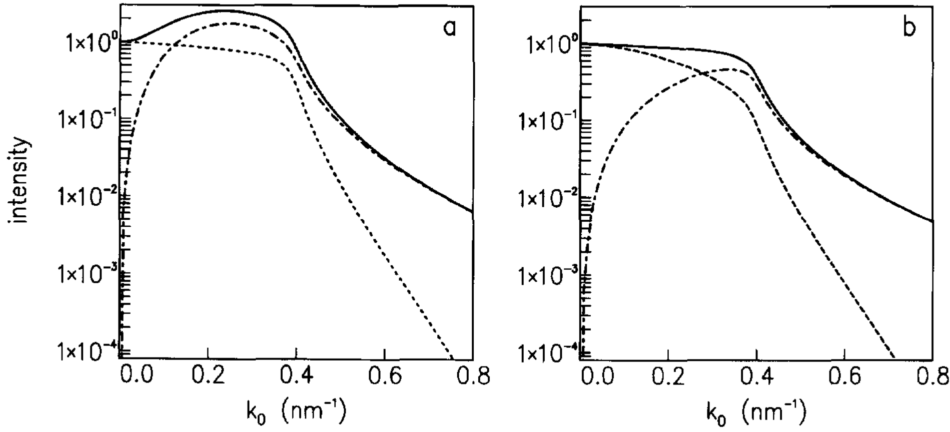

Fig. 3. Reflectivity versus perpendicular incident wave vector for CuKα radiation scattered from a rough platinum sample with rms roughness $\sigma = 1.5$ nm and large lateral correlation length. (a) Calculated using the DWBA: (dashed line) specular reflectivity, Eq. (5); (dot-dashed line) total diffusely reflected intensity from Eq. (7) (relative to incident intensity); (solid line) sum of specular and diffuse reflection. (b) Calculated using Rayleigh approach: (dashed line) specular reflectivity, Eq. (12); (dot-dashed line) total diffusely reflected intensity from Eq. (14) (relative to incident intensity); (solid line) sum of specular and diffuse reflection.

DWBA, but still contains a double sum of structure factors [10, 14].

Eq. (7) and its counterpart for multilayers are widely used to describe diffuse scattering measurements. However, one has to be aware of the limitations. If ξ is large and σ is appreciable, Eq. (7) can give total scattered intensities exceeding the incident intensity, especially in the total reflection region. This is illustrated in Fig. 3(a), showing scattering from a rough platinum surface with $\xi \gg \lambda/(1-\cos\theta)$. Below we will discuss a method which does not give this anomaly.

Eq. (7) describes the diffuse scattering intensity up to $O(k_0^4\sigma^2\xi^2)$, whereas the second- and higher-order terms of Eq. (6) give corrections which are of higher order in $k_0^2\sigma^2$. For the specular case the situation is different. The expressions for the reflection and transmission coefficient obtained from the first-order term of Eq. (6) are, up to $O(k_0^2\sigma^2)$, equivalent to those of Eq. (5). However the second-order term of Eq. (6) also gives a contribution of $O(k_0^2\sigma^2)$ [15], unless $\xi = 0$. Inclusion of this term [16] yields

$$r_k = r_k^0 \exp\left[-2k_0k_1\sigma^2 - \frac{1}{2\pi^2}k_0k^2(1-n^2) \times \int d^2\boldsymbol{p}_\parallel/(p_0+p_1)\tilde{C}(\boldsymbol{p}_\parallel - \boldsymbol{k}_\parallel)\right],$$

$$t_k = t_k^0 \exp\left[(k_0-k_1)^2\sigma^2/2 - \frac{1}{4\pi^2}(k_0-k_1)k^2(1-n^2) \times \int d^2\boldsymbol{p}_\parallel/(p_0+p_1)\tilde{C}(\boldsymbol{p}_\parallel - \boldsymbol{k}_\parallel)\right]. \quad (11)$$

Although within the perturbation-theory approach these expressions are only correct up to $O(k_0^2\sigma^2)$, they are also correct for large $k_0^2\sigma^2$ in the limits of either very small or very large ξ. In the limit $\xi \gg \lambda/(1-\cos\theta)$ the integrals over the power spectral density in Eq. (11) can be performed, yielding

$$r_k = r_k^0 \exp(-2k_0^2\sigma^2),$$

$$t_k = t_k^0 \exp[-(k_0-k_1)^2\sigma^2/2] \quad \text{if } \xi \gg \lambda/(1-\cos\theta). \quad (12)$$

As we will see below, the expressions for this limit can also be obtained in another way.

In Fig. 1 the reflectivity calculated with Eq. (11) is shown for finite ξ, as well as for $\xi \gg \lambda/(1-\cos\theta)$. In the latter case (dot-dashed line) the reflectivity is significantly smaller than that calculated with Eq. (5) (dotted line), whereas for finite ξ (widely dashed line) there is a cross over from one regime to the other.

For multilayers the situation is more complicated, since the second-order contribution of Eq. (6) implies a correlation between the radiation scattered from all interfaces. We have found an expression for the specular reflectivity of a multilayer which is valid for general ξ, but only for small $k_0\sigma$ [17]. If all interfaces are perfectly conformal and all lateral correlation lengths are much larger than $\lambda/(1-\cos\theta)$, a general result is obtained, which will be discussed below.

Now we will take a closer look at the transmitted radiation. Part of it will be absorbed in the sample and this effect can be registered even element specifically by glancing-incidence X-ray fluorescence (GIXRF), i.e. by measuring the X-ray fluorescence (XRF) intensities as a function of incidence angle [18–20]. If an X-ray beam of unit intensity impinges on a sample surface area A at an angle θ, the amount of

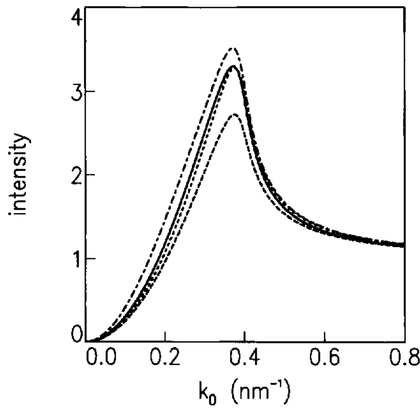

Fig. 4. Absorbed intensity × sin θ/ sin θ_1 versus perpendicular incident wave vector k_0 for CuKα radiation incident on a platinum sample with an rms roughness of 1.5 nm. (Dashed line) no roughness; (dot-dashed line) calculated with flat interfaces as a starting point; (solid line) calculated using error-function graded interface; (dotted line) calculated using new method (see text).

absorbed radiation is

$$T = 1/(A\sin\theta)\int \mathrm{d}^2\boldsymbol{x}\int \mathrm{d}z\,\mu|\phi|^2, \tag{13}$$

where μ is the linear absorption coefficient, the first integral is over the sample surface area A and the second integral over the depth of the sample in which the relevant absorbing atoms are present.

If there is no roughness, the absorption in a bulk sample is $T = |t_k^0|^2 \sin\theta_1/\sin\theta$, where θ_1 is the refraction angle in the sample.

If roughness is present, we have to include the absorption of diffusely scattered radiation, although this effect can be neglected in the limit $\xi \ll \lambda/(1-\cos\theta)$. Another effect is that locally the interface will deviate from the flat position, implying different integration limits in Eq. (13). As an example, Fig. 4 shows $T\sin\theta/\sin\theta_1$ for a bulk sample if $\xi \ll \lambda/(1-\cos\theta)$ (dot-dashed line). In the case without roughness, the dashed line is obtained. We also show the result obtained with the slice method (solid line), which is significantly different. Referring to Fig. 2 we can understand the reason of this discrepancy: in the perturbation theory we used the unperturbed fields (dot-dashed curve) to calculate the absorption in the interfacial region, which clearly is not correct. As we will show now, a better approximate approach is possible. Below we will also discuss the case $\xi \gg \lambda/(1-\cos\theta)$.

In the case of small ξ, a better starting point for the perturbation theory than that of flat interfaces is that where V_0 corresponds to graded interfaces. As we mentioned, however, in the case of an error-function profile Eq. (1) is not exactly solvable. A possible approach is to use another graded profile, e.g. a tangent hyperbolicus, which is exactly solvable [3, 7, 12]. However, this solution is complicated and, moreover, deviates from the error-function profile at large k_0. The slice method, on the other hand, may work well for the above case of absorption, but is not very manageable to calculate diffuse-scattering.

Another possibility is to use an approximate solution for V_0 as a starting point. For instance, one can use the self-consistent fields with the coefficients of Eq. (5). For the diffuse-scattering intensity, this approach would lead to the substitution of the transmission coefficients in Eq. (8) by those of Eq. (5). This formula has also been suggested in the literature [21, 22]. However, from Fig. 2 we see that these fields (dotted line) may deviate even more drastically from the correct ones (solid line) than the unperturbed ones.

We suggest a different approach, assuming that the self-consistent fields are correct except in the interfacial regions. In these regions we simply interpolate continuously between the self-consistent fields at both sides of the interface [17]. The resulting intensity is shown in Fig. 2 (dashed line) and is in good agreement with that obtained using the slice method (solid line). The dotted line of Fig. 4 shows the result for absorption in the case $\xi \ll \lambda/(1-\cos\theta)$. It is seen that the agreement with the slice method is excellent. We found that this approach yields good results for multilayers as well [17].

This approach can also be used to calculate diffuse scattering intensities by using the equations for the multilayer case with in the prefactors the interpolated fields. As an example, in Fig. 5 we compare results for a glancing-incidence rocking curve (see Section 4) of a rough silicon sample. It was assumed that the correlation function of the rough interface can be described by Eq. (15). The results obtained in the two approaches differ significantly, the solid line being for the old approach and the dashed line for the new one. Moreover, it is possible to obtain similar curves in the new approach (dotted line), but with different sets of parameters.

A different approach than the above-mentioned perturbation theory can be used if $\xi \gg \lambda/(1-\cos\theta)$. This is the Rayleigh approach [23], where the interface is considered to be locally flat, so that the field and its derivative can be assumed to be locally continuous. For a single interface the result for the specular case is that the reflection and transmission coefficients are given by Eq. (12). For a multilayer with perfectly conformal interfaces, all having an rms roughness σ, the result also is that the reflection coefficient calculated for flat interfaces has to be multiplied by $\exp(-2k_0^2\sigma^2)$. The transmission coefficient in layer j has to be multiplied by $\exp[-(k_0-k_j)^2\sigma^2/2]$, where k_j is the wave vector in layer j.

For the general case of a multilayer, the calculation of the diffuse-scattering intensity is complicated [24]. For a single

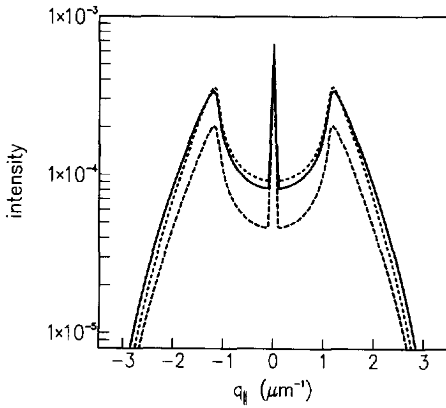

Fig. 5. Scattered intensity (relative to incident intensity) versus parallel wave vector transfer $q_{\|} = k(\cos\theta_d - \cos\theta)$ at constant perpendicular wave vector transfer $q_0 = 0.5\,\mathrm{nm}^{-1}$ for X-rays with $k = 45\,\mathrm{nm}^{-1}$ at a silicon sample with $\sigma = 4\,\mathrm{nm}$. (Solid line) $\xi = 400\,\mathrm{nm}$, $H = 1$, calculated using Eq. (7); (dashed line) $\xi = 400\,\mathrm{nm}$, $H = 1$, calculated using new method; (dotted line) $\xi = 800\,\mathrm{nm}$, $H = 1$, calculated using new method.

interface we found [25] the simple expression

$$\frac{\mathrm{d}\sigma}{\mathrm{d}\Omega} = APS(\boldsymbol{p}_{\|} - \boldsymbol{k}_{\|}, k_0 + p_0) \quad \text{if } \xi \gg \lambda/(1-\cos\theta), \tag{14}$$

that is, an expression very similar to Eq. (7), but with a perpendicular wave-vector transfer $k_0 + p_0$ instead of $k_1 + p_1$.

In Fig. 3(b) we show the results obtained from Eq. (14) for a rough platinum surface with $\xi \gg \lambda/(1 - \cos\theta)$. In contrast to Fig. 3(a), showing results obtained from Eq. (7), now the scattered intensity does not exceed the incident intensity, but the total (diffuse + specular) intensity is equal to that in the case without roughness.

With the same method the transmitted intensity absorbed in the sample can be calculated, using Eq. (13). Now the absorption of the diffusely scattered radiation also has to be taken into account. It is found that the total absorption is equal to that in the case with no roughness (dashed line in Fig. 4). The same results are obtained in the DWBA up to $O(k_0^2\sigma^2)$.

3. The roughness correlation function

In many cases it has been found that an interface can be described as a self-affine fractal over many decades of $\boldsymbol{X}$ [26]. That is, the interface has a fractal dimension $3 - H$, where H is the Hurst parameter ($0 < H < 1$). This parameter can be seen as a jaggedness parameter: for H close to 1 the interface is smooth, whereas for H close to 0 the interface is very jagged. An intersection ("skyline") of the interface, as probed in the case of integration perpendicular to the scattering plane (see Section 4), has dimension $2 - H$. The correlation length ξ can be considered as the upper length scale up to which the interface is fractal.

An often used form for the correlation function [8] is

$$C(\boldsymbol{X}) = \sigma^2 \exp[-(|\boldsymbol{X}|/\xi)^{2H}]. \tag{15}$$

This formula has the right behaviour, with $C(0) = \sigma^2$, and describes fractal behaviour for $|\boldsymbol{X}| \ll \xi$. In the limit $H = 1$ it is a simple Gaussian (which, however, is not fractal), giving a Gaussian power spectral density. For $H = \frac{1}{2}$ it is a simple exponential, leading to $\tilde{C}(\boldsymbol{q}_{\|}) = 2\pi\sigma^2\xi^2(1 + |\boldsymbol{q}_{\|}|^2\xi^2)^{-3/2}$.

There are other functions which also give the right limiting behaviour. An interesting one is the so-called K-correlation function [27–29]:

$$C(\boldsymbol{X}) = B\xi^H |\boldsymbol{X}|^H K_H(|\boldsymbol{X}|/\xi), \tag{16}$$

where B is a constant related to σ (see below), and K_H is the modified Bessel function of order H. (The function proposed in Ref. [28] uses a slightly different definition of the constants B and ξ.) The corresponding power spectral density is $\tilde{C}(\boldsymbol{q}_{\|}) = \tilde{C}(0)(1 + |\boldsymbol{q}_{\|}|^2\xi^2)^{-1-H}$. For $H = \frac{1}{2}$ this is equivalent to that following from Eq. (15). If there is no lower cut-off length for $C(\boldsymbol{X})$, the relation between σ and B is $\sigma^2 = B\xi^{2H}2^{H-1}\Gamma(1 + H)/H$ and $\tilde{C}(0) = 4\pi H\sigma^2\xi^2$. In the limit $H = 0$, Eq. (16) diverges logarithmically for small $\boldsymbol{X}$. We will assume that the interface has a smallest constituting element (atom or cluster) of size x_0. Then one finds $\sigma^2 = \frac{1}{2}B\ln(1 + \xi^2/x_0^2)$ and $\tilde{C}(0) = 2^{3/2}\pi\xi^2 B$. Generalising to $H \neq 0$ and taking a correlation function with x_0 as lower cut-off length, one obtains $\sigma^2 = B\xi^{2H}2^{H-1}\Gamma(1 + H)/H[1 - (1 + \xi^2/x_0^2)^{-H}]$ and $\tilde{C}(0) = 2^{1+H}\pi\Gamma(1 + H)B\xi^{2+2H}$.

The above model is in agreement with existing models for film growth [26]. For $H \neq 0$ and $(x_0/\xi)^{2H} \ll 1$, we have $\sigma \sim \xi^H$ and both ξ and σ can be assumed to increase with the film thickness t according to power laws. For $H = 0$ and $x_0/\xi \ll 1$, we have $\sigma^2 \sim \ln\xi$. Assuming again a power-law growth for ξ with t, we find $\sigma^2 \sim \ln t$, in agreement with the well-known Edward–Wilkinson growth model [30].

These considerations seem to give the K-correlation function, Eq. (16), more physical justification than Eq. (15). However, for small H values, Eq. (15) yields a more cusp-like structure factor than Eq. (16), which we found often to be in better agreement with experimental data.

For a multilayer we also need the correlation function C_{ij} between the roughnesses of different interfaces. In the Edward–Wilkinson model [31] one can derive

$$\tilde{C}_{ij}(\boldsymbol{q}_{\|}) = \tilde{C}_{j>}(\boldsymbol{q}_{\|})\,\tilde{c}_{ij}^{\perp}(\boldsymbol{q}_{\|}), \tag{17}$$

where $j>$ denotes the interface i or j which is closest to the substrate and $\tilde{c}_{ij}^{\perp}$ is the replica factor for the roughness. In general, the replica factor will decrease with increasing lateral frequency $\boldsymbol{q}_{\|}$. Often, however, a simple

frequency-independent form is appropriate: $\tilde{c}_{ij}^{\perp}(\boldsymbol{q}_{\|}) = c_{ij}^{\perp} = \exp(-d_{ij}/\xi_{\perp})$, where d_{ij} is the distance between interfaces i and j and $\xi_{\perp}$ is the perpendicular correlation length. It is important to note that not all parameters can be chosen independently (see Note 43 of Ref. [32]).

Other correlation functions given in the literature often have a more phenomenological character. For instance, for an ion-etched molybdenum–silicon multilayer it was found that $C(\boldsymbol{X}) = 1/(1 + |\boldsymbol{X}|^2/\xi_{\text{eff}}^2)$, with a $q_{\perp}$-dependent ξ_{eff}, can give a good description of the measured data [33].

Furthermore, as was indicated above, one can obtain an estimate of $C(\boldsymbol{X})$ by Fourier transforming the measured data if interference effects can be neglected. For instance, this method has been applied for a gold film on GaAs [34]. Finally, as discussed in Section 2, in some cases it may be more appropriate to express the structure factor in another way than using the correlation function.

4. Scattering geometries

The set-up which is most often used for X-ray scattering experiments has a geometry where the detector is located in the scattering plane, i.e., the plane formed by the incident wave vector and the normal to the sample. In most cases, both the sample and the detector can be rotated to change the incidence angle and the detection angle. (Instead of a rotatable detector also a position-sensitive detector can be used to obtain information as a function of detection angle.) The divergence of both incident and detected beam is typically $\Delta\theta \simeq 3 \times 10^{-4}$ and the resolutions in reciprocal space are $\Delta k_0 \simeq k\Delta\theta$ and $\Delta k_{\|} = k_0\Delta\theta$.

Often a slit is placed before the detector which is long in the direction perpendicular to the scattering plane. In that case the measured diffusely scattered intensity is integrated over the perpendicular direction. Denoting this direction by y, the diffusely scattered intensity for a single interface is proportional to

$$\int \mathrm{d}q_y\, S(\boldsymbol{q}_{\|}, q_{\perp}) = 2\pi\, |\exp(-q_{\perp}^2\sigma^2/2)/q_{\perp}|^2 \times \int \mathrm{d}^2X \exp(\mathrm{i}q_{\|}X)\{\exp[|q_{\perp}|^2 C(X)] - 1\},$$

where Eq. (9) was used.

For small $q_{\perp}\sigma$ this is proportional to $\tilde{C}(q_{\|}) = \int \mathrm{d}X \exp(\mathrm{i}q_{\|}X)\, C(X)$, the Fourier transform in the scattering plane of the one-dimensional correlation function $C(X)$. Note that $C(X)$ may differ in different directions along the sample surface. Examples are machined surfaces [19] and interfaces with steps in one direction [11, 35].

Close to the specular condition one will measure the sum of true specular reflection and diffuse scattering. If the specular reflectivity is fitted, the diffuse scattering should be subtracted. In principle, the ratio of the diffuse scattering intensity to the specular contribution contains relevant information on correlation lengths, etc. In practice, it is difficult to obtain this very accurately, since it is determined by the details of the optics of the instrument, which is influenced by the size and flatness of the sample.

The diffuse scattering can be measured in various possible scans. In a rocking (or transverse) scan both the source and the detector are fixed, whereas the sample is rocked from zero incidence angle to zero detection angle. In such a scan the perpendicular wave vector transfer $q_0 = p_0 + k_0$ is essentially constant. If the angle between the incident beam and the detected beam is 2θ, length scales down to $\lambda/(1 - \cos\theta)$ are probed. An example of such a scan was given in Fig. 5.

Other possible scans are: an offset scan, i.e. a coupled scan of sample and detector with the angle between detected beam and sample surface equal to the incidence angle plus an offset angle; a detector scan, where only the detection angle is scanned at fixed sample and source positions; a source scan, where the incidence angle is scanned at fixed sample and detector positions. A complete mapping of the scattered intensity results in a reciprocal-space map, i.e., a contour plot of constant intensities in the $q_{\|}$–q_0 plane. An example will be given in Fig. 6.

A larger part of reciprocal space can be probed if the detector can move out of the scattering plane, as in glancing-incidence diffraction [36]. In that case it is possible to reach larger $|\boldsymbol{q}_{\|}|$ values and $C(\boldsymbol{X})$ can be probed down to smaller values of $|\boldsymbol{X}|$ [37]. Moreover, if it is assumed that the Born approximation is valid, $C(\boldsymbol{X})$ can be obtained by Fourier transformation of the diffuse-scattering intensities, provided that $C(0)$ is known, e.g. from the specular data [37].

5. Example

An example of an experiment for which we were able to describe the diffuse-scattering data and to extract material parameters, is shown in Fig. 6. These data, measured with the detector in the scattering plane, are for a multilayer consisting of 20 periods of approximately 10 nm magnetite (Fe_3O_4) and approximately 3 nm magnesium oxide on a magnesium aluminate substrate [38]. From a fit of the specular reflectivity we found that between the Fe_3O_4 and MgO layers intermixed layers are formed, presumably consisting of $MgFe_2O_4$. The influence of the roughness on the specular scattering was described using Eq. (5). We found $\sigma = 0.6$ nm for most interfaces, whereas the top interfaces are slightly rougher.

In the reciprocal-space map of Fig. 6 the vertical line $q_{\|} = 0$ denotes the specular scan, with the total-reflection region up to $q_0 \simeq 0.45\ \text{nm}^{-1}$ and the first three multilayer Bragg peaks at $q_0 \simeq 0.64$, 1.05 and 1.51 nm^{-1}. The white regions,

left and right, are part of the hemicircles which cannot be reached in reflection geometry.

In the diffuse-scattering distribution we see two kinds of structure: circle-like ridges approximately parallel to those hemicircles and banana-shaped sheets through the Bragg peaks. The former ridges are due to interference effects arising from the prefactors in the formulas for diffuse scattering. It is well known that, if either the incident angle or the detection angle equals the critical angle for total reflection, an enhanced diffuse scattering is seen ("Yoneda wings" [39]), since the transmission coefficients in Eq. (8) are maximum at the critical angle. In Fig. 6 this phenomenon gives rise to the circle-like ridges crossing the line $q_{\|} = 0$ at $q_0 \simeq 0.45\ \mathrm{nm}^{-1}$. Similar ridges are crossing the line $q_{\|} = 0$ in the first Bragg peak (those corresponding to higher-order Bragg peaks have a too low intensity to be seen here). Along these lines either the incident or the detection angle is close to the Bragg angle, resulting in a severe modulation of the prefactors. A similar phenomenon is present for one or a few layers on a substrate. Then the specular reflectivity exhibits Kiessig fringes. In the diffuse scattering a corresponding modulation of the intensity is seen [32, 40].

It is interesting to realise that the angle can be tuned to give less or more intensity at a particular set of interfaces. This provides a tool to distinguish between the roughness of different interfaces. In the underlying case we found that all interfaces can be described with the same parameters (apart from the higher rms roughness for the top interfaces).

The banana-shaped sheets are due to perpendicular correlation in the multilayer [13, 14, 41]. In the case that $c_{ij}^{\perp} = 0$, they are absent. Qualitatively, they can be understood as follows: if the incidence angle with respect to the average interfaces does not equal a Bragg angle, part of the rough interfaces yet may be at the Bragg angle. If the successive rough interfaces are highly conformal, the waves scattered by the mentioned part of the interfaces can interfere constructively. This implies that the wave vector transfer in the sample obeys the Bragg condition. This yields essentially horizontal sheets which, because of refraction, are bended upwards.

From Fig. 6 we found that for this sample we can assume $c_{ij}^{\perp} = 1$ for all interfaces, implying that the perpendicular correlation length is larger than the thickness of the whole multilayer stack.

We were able to simulate the data of Fig. 6 by assuming furthermore that all interfaces have the same lateral correlation length ξ and the same Hurst parameter H. Good agreement with experiment was obtained with $\xi = 100$ nm and $H = 0.3$ [38]. For the calculation we used the formulas valid for small ξ. Indeed, in the region where the intensity is high enough to make a comparison, we have $\xi \lesssim \lambda/(1-\cos\theta)$.

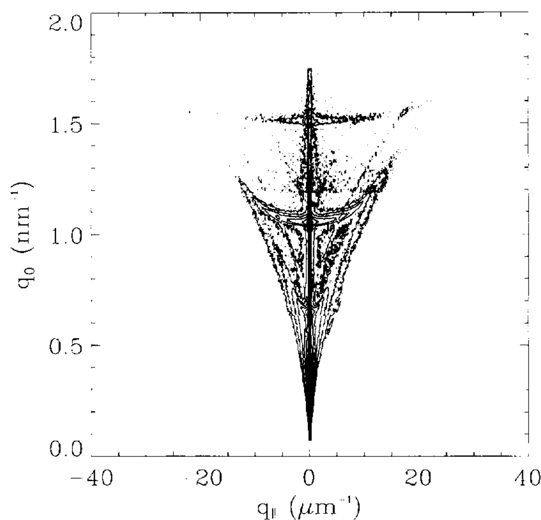

Fig. 6. Reciprocal-space map showing contours of constant intensity measured for scattering of CuKα radiation from a multilayer consisting of 20 periods of Fe_3O_4 and MgO on $MgAl_2O_4$.

6. Conclusions

In Section 2 we gave an overview of scattering theories, from which the following can be concluded. If ξ is not too large, which in practice often is the case, Eq. (5) can be used for specular reflection and transmission, also for each interface in a multilayer. If ξ is large, Eq. (12) has to be applied. In the case of intermediate ξ, Eq. (11) can be used for the specular reflection and transmission by a single interface. For multilayers only approximate formulas are available [17], valid if $k_0\sigma$ is small.

To calculate diffuse scattering for the case of not too large ξ, Eq. (7) and its counterpart for multilayers can be used if $k_0\sigma$ is not too large. Otherwise the new description discussed above is applicable. In the case of large ξ, the diffuse scattering is described by Eq. (14) for a single interface. For a multilayer, approximate numerical methods valid in this limit are given in the literature [24]. Up to now, no general method is available to calculate diffuse scattering at intermediate ξ. In the case that interference effects can be neglected, the Born approximation can be used [8, 14].

Possible forms for the roughness correlation function were described in Section 3. We indicated that there are several ways to describe self-affine fractal interfaces, which may give somewhat different results. Because of the various scattering theories, the competing forms for the correlation function and experimental uncertainties (cf. Section 4), we believe that the obtained values of ξ in general have an uncertainty of about a factor of two. Also the H values probably have to be considered as indicative. The rms-roughness values can be determined much more accurately, especially

in the case of small ξ. Despite the uncertainties, valuable information on the nature of interface roughness can be obtained by X-ray scattering measurements, for instance, in the example of Section 5.

References

[1] H. Zabel and I.K. Robinson (eds.), Surface X-Ray and Neutron Scattering (Springer, Berlin, 1992).
[2] H.J. Lauter and V.V. Pasyuk (eds.), Proc. Internat. Conf. on Surface X-Ray and Neutron Scattering SXNS-3, Physica B 198 (1994).
[3] S. Dietrich and A. Haase, Phys. Rep. 260 (1995) 1.
[4] L.G. Parratt, Phys. Rev. 95 (1954) 359.
[5] L. Névot and P. Croce, Revue Phys. Appl. 15 (1980) 761.
[6] R. Pynn, Phys. Rev. B 45 (1992) 602.
[7] A. Caticha, in: Physics of X-Ray Multilayer Structures, 1994, Technical Digest Series, Vol. 6 (Optical Society of America, Washington, DC, 1994) p. 56; A. Caticha, Phys. Rev. B 52 (1995) 9214.
[8] S.K. Sinha, E.B. Sirota, S. Garoff and H.B. Stanley, Phys. Rev. B 38 (1988) 2297.
[9] B. Vidal and P. Vincent, Appl. Opt. 23 (1984) 1794.
[10] S.K. Sinha, J. Phys. III 4 (1994) 1543.
[11] S.K. Sinha, M.K. Sanyal, S.K. Satija, C.F. Majkrzak, D.A. Neumann, H. Homma, S. Szpala, A. Gibaud and H. Morkoc, Physica B 198 (1994) 72.
[12] A.V. Andreev, A.G. Michette and A. Renwick, J. Modern Opt. 35 (1988) 1667.
[13] V. Holý, J. Kuběna, I. Ohlídal, K. Lischka and W. Plotz, Phys. Rev. B 47 (1993) 15 896; V. Holý and T. Baumbach, Phys. Rev. B 49 (1994) 10 688; V. Holý, J. Kuběna, W.W. van den Hoogenhof and I. Vávra, Appl. Phys. A 60 (1995) 93.
[14] M.K. Sanyal, S.K. Sinha, A. Gibaud, S.K. Satija, C.F. Majkrzak and H. Homa, p. 91 in Ref. [1].
[15] V.K. Ignatovich, The Physics of Ultracold Neutrons (Clarendon Press, Oxford, 1990) App. 6.10.
[16] D.K.G. de Boer, Phys. Rev. B 49 (1994) 5817.
[17] D.K.G. de Boer, Phys. Rev. B, in press.
[18] D.K.G. de Boer, Phys. Rev. B 44 (1991) 498.
[19] W.W. van den Hoogenhof and D.K.G. de Boer, Spectrochim. Acta 48B (1993) 277.
[20] D.K.G. de Boer, A.J.G. Leenaers and W.W. van den Hoogenhof, X-Ray Spectrom. 24 (1995) 91.
[21] W. Weber and B. Lengeler, Phys. Rev. B 46 (1992) 7953.
[22] M. Kopecky, J. Appl. Phys. 77 (1995) 2380.
[23] J.W. Strutt (Baron Rayleigh), The Theory of Sound (Macmillan, London, 1896; 2nd edn.) §272a.
[24] J.M. Eastman, Phys. Thin Films 10 (1978) 167.
[25] D.K.G. de Boer, Phys. Rev. B 51 (1995) 5297.
[26] P. Meakin, Prog. Solid State Chem. 20 (1990) 135.
[27] E.L. Church and P.Z. Takacs, SPIE 645 (1986) 107; 1530 (1991) 71.
[28] G. Palasantzas, Phys. Rev. B 48 (1993) 14 472.
[29] D.K.G. de Boer, A.J.G. Leenaers and W.W. van den Hoogenhof, J. Phys. III 4 (1994) 1559.
[30] S.F. Edwards and D.R. Wilkinson, Proc. Roy. Soc. London A 381 (1982) 17.
[31] E. Spiller, D. Stearns and M. Krumrey, J. Appl. Phys. 74 (1993) 107.
[32] J.-P. Schlomka, M. Tolan, L. Schwalowsky, O.H. Seeck, J. Stettner and W. Press, Phys. Rev. B 51 (1995) 2311.
[33] R. Schlatmann, J.D. Shindler and J. Verhoeven, Phys. Rev. B 51 (1995) 5345.
[34] D.Y. Noh, Y. Hwu, H.K. Kim and M. Hong, Phys. Rev. B 51 (1995) 4441.
[35] W.W. van den Hoogenhof and D.K.G. de Boer, Mater. Sci. Forum 143–147 (1994) 1331.
[36] H. Dosch, Critical Phenomena at Surfaces and Interfaces, Springer Tracts in Modern Physics 126 (Springer, Berlin, 1992).
[37] T. Salditt, T.H. Metzger, C. Brandt, U. Klemradt and J. Peisl, Phys. Rev. B 51 (1995) 5617; T. Salditt, to be published.
[38] D.K.G. de Boer, A.J.G. Leenaers and R.M. Wolf, J. Phys. D: Appl. Phys. 27 (1995) A227.
[39] Y. Yoneda, Phys. Rev. 113 (1963) 2010.
[40] D.K.G. de Boer, A.J.G. Leenaers and W.W. van den Hoogenhof, Appl. Phys. A 58 (1994) 169.
[41] D.E. Savage, J. Kleiner, N. Schimke, Y.-H. Phang, T. Jankowski, J. Jacobs, R. Kariotis and M.G. Lagally, J. Appl. Phys. 69 (1991) 1411.